Photoacoustic Imaging Assisted Radiofrequency Ablation: Illumination Strategies and Prospects

Kalloor Joseph Francis, Elina Rascevska and Srirang Manohar
Biomedical Photonic Imaging Group, and Multimodality Medical Imaging Group,
Faculty of Science and Technology, Technical Medical Center University of Twente,The Netherlands
f.kalloorjoseph@utwente.nl

***Abstract*—Surgical resection is considered the gold standard for tumor treatment with curative intent. However, in most cases, patients are not eligible for resection, especially in functional tissue like liver. Minimally invasive thermal treatment like Radiofrequency Ablation (RFA) is gaining more applicability in this scenario. The success of RFA treatment depends on accurate needle placement and complete tumor ablation. Widely used Ultrasound (US) imaging lacks in providing accurate feedback of RFA device location and ablated tissue boundary. Here we propose Photoacoustic (PA) imaging in combination with US imaging for RFA device guidance and in differentiating ablated tissue. We employ two illumination strategies for PA imaging: an extracorporeal light delivery, and an interstitial light delivery. First, using the extracorporeal illumination we demonstrate how PA imaging can improve RFA device visibility and in differentiating ablated tissue in an *ex vivo* laboratory setting. Further, we expose the difficulty in imaging highly absorbing tissue using illumination from the surface of the skin. This limitation leads to the development of an interstitial illumination probe. We compare these two illumination strategies and present our preliminary results in RFA device guidance using the interstitial probe. Our results show the potential of PA imaging in improving the accuracy of the RFA procedure.**

***Index Terms*—Photoacoustic imaging, Radiofrequency ablation, Ultrasound imaging, Interstitial illumination, Thermal treatment, *ex vivo*.**

I. Introduction

The liver is considered as a tumor prone site for both primary and metastases. Historically, resection of the malignant tumor can result in a long term survival and hence considered as the treatment of curative intent. However, more than 70% of the patients are not eligible for surgical resection as the remnant liver should exceed a minimum of 25% [1]. Locoregional ablation of the tumor has gained popularity in the past decade as a potential alternative to surgical resection [2]. Although there are many options for tumor ablation including the use of microwave and cryoablation, RFA is the clinically preferred modality, as the morbidity and mortality are low compared to other methods [3], [4]. In the RFA procedure, alternating current is applied across a needle electrode which is introduced into the tumor volume and a grounding pad with a larger surface attached to the surface of the skin. Alternating current (350 - 500 kHz) induces friction heat due to ionic agitation around the needle which conducts the tissue ablating the tumor volume [5].

The main limitation of RFA is the high tumor recurrence due to incomplete ablation [6]. There are two reasons for the incomplete tumor ablation. First is the intrinsic heating mechanism of RFA. As resistive heating in the proximity of the RFA needle is faster than conductive heating to the surrounding tissue, this can cause desiccation and abrupt increase in impedance [2]. However, there are developments in the RFA device design with multiple electrodes and cooled tips to overcome this limitation [7]. The second aspect is insufficient feedback from the imaging modality guiding the procedure. Although Magnetic Resonance Imaging (MRI) and Computed Tomography are used for RFA procedures, due to the real-time nature and the possibility to use in an outpatient setting, US imaging is the popular choice. The tumor recurrence varies from 2% to 60% for US assisted RFA procedures. Studies show that when smaller the tumor and close to the US transducer, the chances of local recurrence is less while for larger and distant from the transducer chances of recurrence are high [8]. The US imaging depends on the specular reflection from the needle for guidance and bubble formation to monitor the ablation. The deeper the tumor, the steeper is the angle that the RFA needle needs to make which makes it difficult to visualize under US imaging. Additionally, the larger the tumor, the more challenging and inaccurate the assessment of bubble formation can becomes, which could result in incomplete ablation. Hence, there is a need for a new modality which can work alongside with US imaging providing more accurate feedback for the RFA procedure.

Photoacoustic (PA) imaging can be a potential solution to tackle the above limitations of US imaging. In PA imaging, pulsed light induces thermoelastic expansion at optically absorbing sites, resulting in a local pressure rise which can be detected using US transducers to form a pressure map [9]–[11]. PA imaging can be potentially used for RFA procedure because of three reasons (i) optical absorption of metal needle is high compared to tissue resulting in high contrast [12], [13] (ii) optical properties of tumor is different from normal tissue which enables targeting [14] and (iii) ablated and native tissue differ in their optical properties [15], [16]. Previous work also showed that PA imaging can differentiate ablated and native cardiac tissue [15], [17], [18]. However, imaging a percutaneous RFA procedure requires a combination of the

This work is funded by a joint grant from the Netherlands Organisation for Scientific Research (NWO)/the Netherlands Organisation for Health Research and Development (ZonMw) and the Department of Biotechnology (Government of India)

978-1-7281-1895-6/19/$31.00

above three aspects [19]–[21].

In this work, we propose PA imaging for percutaneous RFA procedure, specifically for needle guidance and ablation imaging. We compare two illumination strategies, one from the surface of the skin and light delivered through optical fiber inside the tissue. We present our preliminary results and discuss the prospects of PA imaging in RFA procedures.

II. Methods

The *ex vivo* experimental setup was designed such that both imaging and ablation can be performed simultaneously. The setup consists of pulsed laser and ultrasound imaging system for imaging, custom-developed fiber bundles for light delivery, RF generator and electrodes for ablation and a glass tank with metal base for holding the tissue sample. Fig. 1 shows the schematic of the experimental system.

A. Experimental Setup

1) Light Delivery: For PA imaging pulsed light from an Nd:YAG Q-switched laser (Spectra-Physics, USA) was used together with an OPO (versaScan L-532,GWU, Germany) for wavelength tuning. We used two illumination methods. The output from the OPO is first passed through ND filters to reduce the energy and then directed to either extracorporeal illumination fiber bundle or the annular fiber probe using a flip mirror. In the extracorporeal illumination, the fiber bundle splits into seven subbundles of 4 mm diameter. A 3D printed fiber holder was designed to hold six fibers on either side of the US transducer as shown in Fig. 1 (b) such that the beams from the fibers intersect at the focus of the transducer (20 mm). The measured pulse energy from the six fibers was 9.2 mJ at 720 nm, resulting in an exposure of 11.8 mJ/cm^2 which is less than the permissible limit of 20 mJ/cm^2 [22].

A custom made annular fiber probe was used for interstitial illumination (Fig. 1 (d)). The probe consists of two steel ferrules with 72 fibers (100 μm, NA 0.2) arranged between them. The inner ferrule is designed to accommodate 14 gauge interventional needle in its lumen. The diameter of the whole probe is 3.4 mm and with a length of 80 mm. The pulse energy of 1.5 mJ at 720 nm was used for interstitial illumination. Although the exposure is more than the permissible limit for skin, for interstitial illumination these limits are not defined yet.

2) Imaging:: PA and US imaging were simultaneously performed using a research ultrasound system Alpinion Ecube 12R (Alpinion Medical Systems, South Korea). A custom imaging sequence was used for combined imaging. An external synchronization pulse from the laser marks the starting of PA signal acquisition in the receiver only mode followed by a 20 ms waiting time and a focused B-mode US imaging. Built-in real-time reconstruction was used for both PA and US image formation [23].

3) Ablation system:: A clinical RFA system from Angiodynamics (USA) was used for the experiments. The system consists of an RF generator (1500X, 460 kHz) and two unipolar electrodes. One a needle electrode (Fig 1 (c)) (StarBurst XL) and a dispersive pad. A custom-developed tank with metal base was used to hold the tissue sample. The metal base also enabled grounding with the dispersive electrode attached to its bottom as shown in Fig. 1 (a).

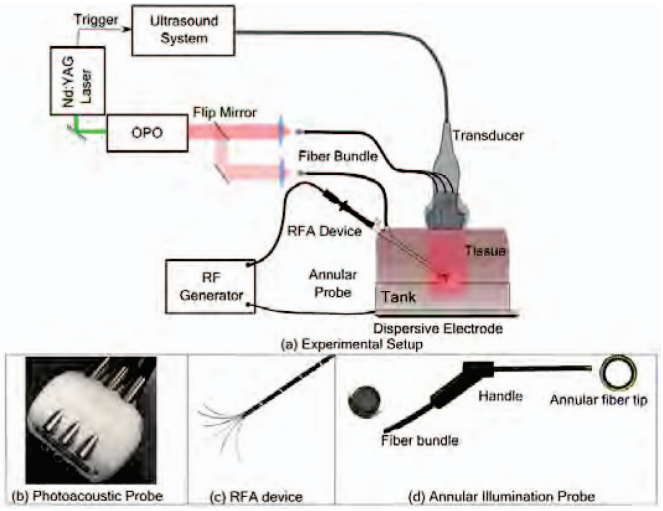

Fig. 1. Combined photoacoustic/ultrasound imaging and radiofrequency ablation (RFA) system. (a) Experimental setup for simultaneous ablation and imaging. (b) Photoacoustic probe with extracorporeal illumination and linear transducer array for detection. (c) Multi-electrode RFA device. (d) Annular fiber probe for interstitial illumination.

B. Procedure

1) Needle guidance:: PA assisted RFA needle guidance experiments were performed on *ex vivo* chicken and bovine liver tissue. The tissue samples were obtained from a local butcher and stacked in the tank. In the first experiment, extracorporeal illumination was used and the RFA needle was inserted at 0^0 and 30^0 with respect to the transducer array. PA and US images of the needle and multiple electrodes (tines) were made. The contrast to noise ratio (CNR) of the images were computed using $|\mu_{ROI} - \mu_{Bck}|/\sqrt{\sigma^2_{ROI} + \sigma^2_{Bck}}$, where μ is mean and σ is the standard deviation of pixels. In the second experiment, the RFA needle was inserted to the liver through a layer of chicken tissue mimicking a percutaneous procedure. The tines were deployed into the liver sample and the depth sensitivity of PA imaging is measured.

In the third experiment needle guidance to a target tissue using both extracorporeal and interstitial illumination were compared. The target tissue was prepared by immersing chicken tissue in India ink. The target was then placed between slices of chicken breast tissue to obtain two different imaging depths. Combined PA and US images of the sample were made. The signal to noise ratio of the target was calculated and compared for both illumination methods. In the fourth experiment, visualizing RFA needle placed through the annular probe was imaged with interstitial illumination PA imaging. The goal was to understand how well the multi-tined RFA needle can be visualized using interstitial illumination in an *ex vivo* setting.

2) Ablation imaging:: A final experiment was conducted to understand how the PA intensity differs for ablated and native tissue. A thin slice (5 mm) of a bovine liver was extracted and mounted on a polyethylene (Saran™) film in Phosphate-buffered saline (1X PBS) and Intralipid solution. The intralipid was used to diffuse the light from the extracorporeal illumination probe, while PBS was used to keep the tissue intact. Laser wavelength was tuned to 760 nm with a pulse energy of 8.6 mJ. The specific wavelength was chosen to target absorption from blood in the liver sample. PA and US C-Scan images were obtained by stepping the probe along its short axis with a step size of 1 mm covering an area of 25 mm. The images were combined and maximum intensity projection was obtained.

III. Results and Discussion

In this section we present our results on PA assisted RFA needle guidance and compare it with US imaging. Starting with less absorbing tissue we advance to more absorbing liver tissue and analyze the change in imaging depth using extracorporeal illumination. We then compare both extracorporeal and interstitial illumination and finally present imaging of ablated liver tissue.

Figure 2 shows the RFA needle inserted at two different angles (0^0 and 30^0) and the corresponding PA and US images. It can be observed that the contrast of the US images dropped drastically with angle. In RFA needle deployment the trocar, as well as the tines, must be visible to estimate the treatment volume. To understand how the US and PA images differ, CNR values were extracted over a patch of 6x6 mm region of interest in the trocar and tines to a background slice of the same size. When the RFA needle was placed parallel to the transducer maximum contrast was obtained. CNR for the trocar of the needle in US image was 1.9±0.03 and for tines, it was 1.4±0.04, while for PA image CNR values were 5.1±0.2 and 8.9±0.06 respectively. The change in contrast at 30^0 is evident in the CNR values, with US images being low as 0.1±0.04 for the trocar and 0.7±0.06 for the tines. No significant contrast drop was observed for PA imaging, with CNR of 3.8±0.13 and 6.0±0.2 respectively for trocar and tines. However, there are reconstruction artifacts in PA imaging which resulted in a small change in its contrast. The key difference in the contrast is because of the specular reflection in US imaging resulting in acoustic waves escaping the transducer aperture, while PA signals can still be captured even at a steeper angle.

Percutaneous RFA procedures demand imaging of tissue several centimeters from the surface. However, in highly absorbing tissue such as liver, the penetration of light can be limited. Figure. 3 shows PA imaging of RFA needle inserted into a liver tissue using extracorporeal illumination. The total achieved penetration depth through the soft tissue and the liver is 16.7 mm with 9.4 mm in soft tissue and 7.3 mm the liver. This limits the applicability of extracorporeal illumination to less absorbing tissue like breast or kidney for ablation while there is a need for another illumination for highly absorbing tissue.

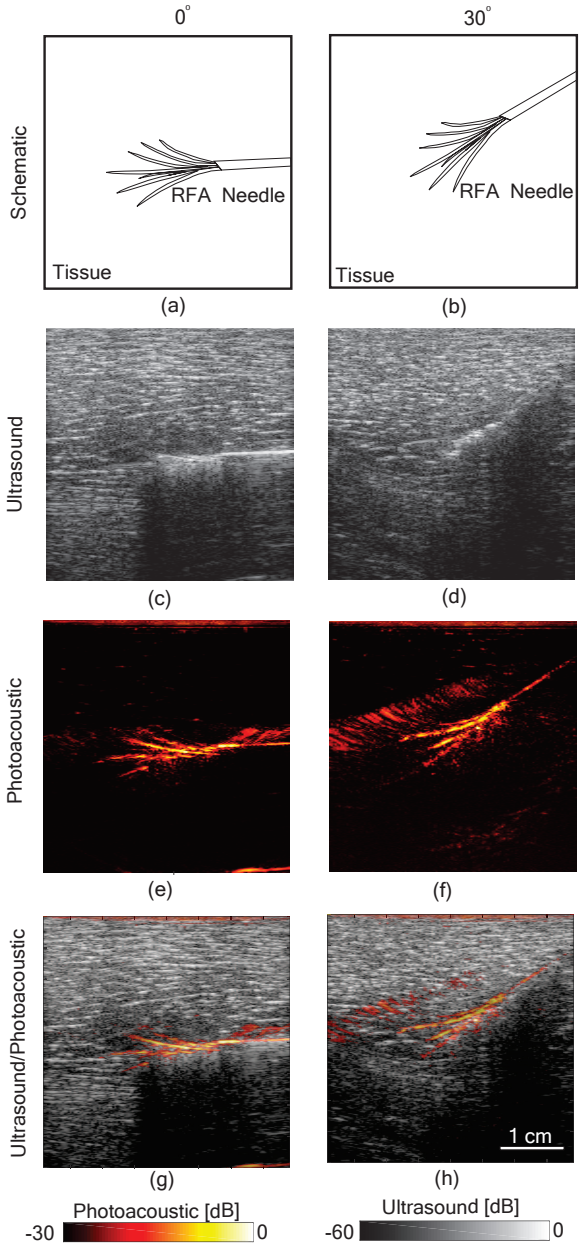

Fig. 2. RFA needle visualization at 0^0 and 30^0. (a-b) shows the schematic, (c-d) ultrasound image, (e-f) photoacoustic image and (g-h) is the combined image. (Reproduced with permission of the authors and publishers.)

Results using an interstitial illumination is presented in Fig. 4. Here we compare both extracorporeal and interstitial illumination in guiding the needle to an absorbing target placed at two different depths. SNR values were calculated between the target and the background. For the target at 15 mm, an SNR of 26.8 was observed for interstitial and 10 for extracorporeal illumination. However, for a deeper target at 32 mm, SNR values were 19.5 for interstitial and 7.2 for extracorporeal illumination. From the SNR values, it is evident that interstitial illumination using an annular probe can be used to guide the

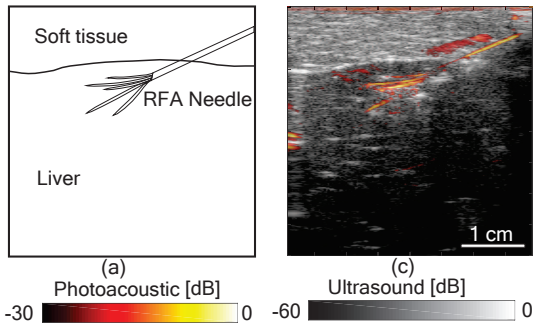

Fig. 3. Photoacoustic assisted RFA needle guidance to liver. (a) Schematic of the imaging plane showing soft tissue, liver and needle location. (b) Combined photoacoustic and ultrasound image. (Reproduced with permission of the authors and publishers.)

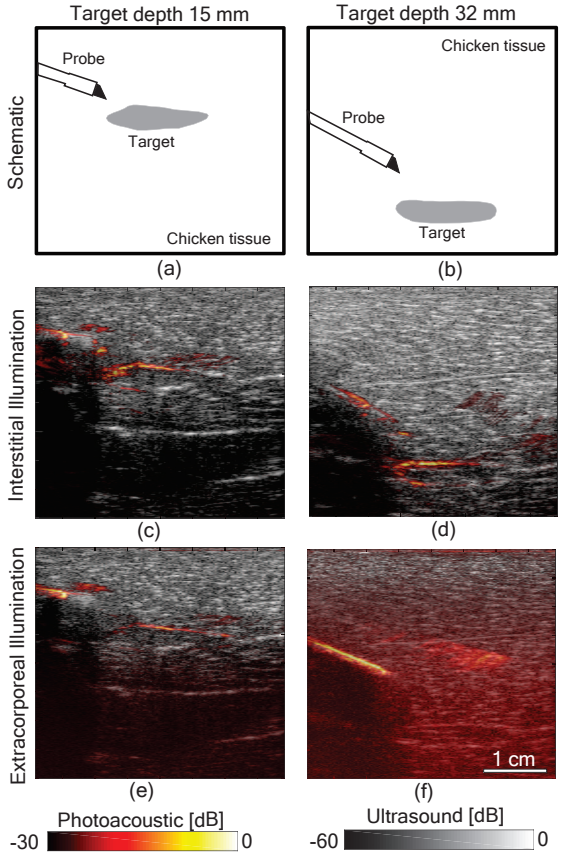

Fig. 4. Comparison between interstitial and extracorporeal illumination. (a) and (b) showing the schematic with absorbing target at 15 mm and 32 mm respectively. (c) and (d) are the combined photoacoustic and ultrasound images obtained using interstitial illumination. (e) and (f) are the combined photoacoustic and ultrasound images obtained using extracorporeal illumination.

RFA needle to a deeper target.

Figure. 5 shows our preliminary experiment on visualizing the RFA needle in an *ex vivo* tissue using the interstitial illumination probe. Our first observation is that it is possible to image multiple tines using the proposed illumination method.

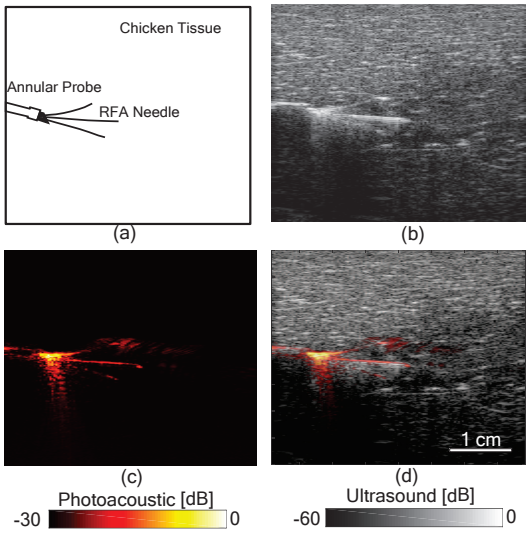

Fig. 5. RFA Needle visualization. (a) Schematic of the RFA needle inserted through the annular probe into the tissue. (b) Ultrasound image of the tissue and the needle. (c) Photoacoustic image obtained using interstitial illumination and (d) the combined image. (Reproduced with permission of the authors and publishers.)

We observed a CNR of 8.2±0.3 for PA image and 1.1±0.2 for US image, taking the RFA needle as the region of interest. However, there is also a limitation, the light was absorbed heavily by the metallic part of the RFA needle at the vicinity of the fiber tip, resulting in a high PA signal from that region. This high PA signal creates artifacts and also obscure the structures located away from the fiber. To solve this problem we are working on an approach to spread out the light exiting the fiber to a larger volume.

In the final experiment, an ablated bovine liver tissue was imaged. Figure. 6 shows the photograph of the sample and US and PA maximum intensity projected image. The line profiles taken from the center of ablation for both US and PA is shown in Fig. 6 (d). PA intensity differs by 5.2±0.5 dB for PA imaging. While observed PA intensity was low for ablated tissue compared to native, carbonized tissue at the center of the ablation gave a high PA signal which is 1.9±0.6 dB higher than that of ablated tissue. In ultrasound imaging, the ablated tissue boundary is not visible.However, it shows the tissue structure and the hole made by the trocar.

Our preliminary study has some limitations. Firstly, there are reconstruction artifacts in the PA images. We are investigating the source of the artifact and methods to remove them. Secondly, ablated tissue imaging is performed on a thin slice for the first experiment. We are developing methods to perform the same in deep tissue. Due to the reduction in absorption with thermal treatment a new contract mechanism is needed to differentiate ablation in deep tissue.

IV. Conclusion

Our preliminary results are promising. It shows that Photoacoustic (PA) imaging can be a potential modality to guide

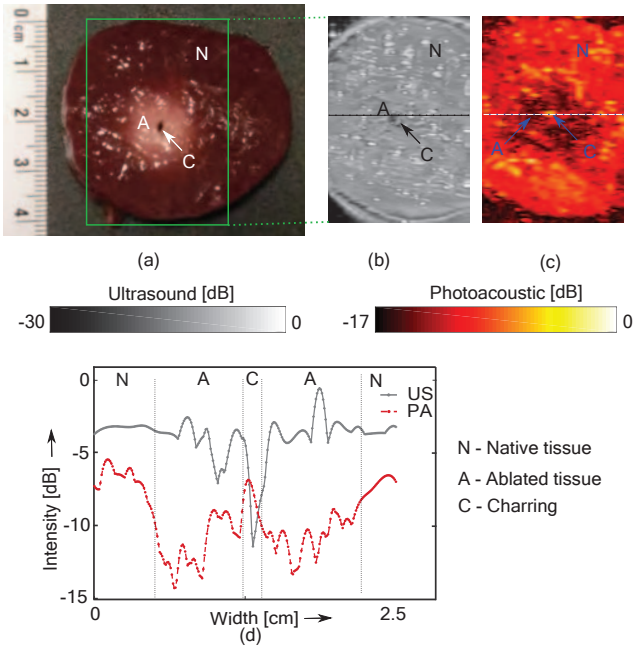

Fig. 6. Ablated tissue imaging. (a) Photograph of the ablated liver tissue. (b) Ultrasound Maximum Intensity Projection (MIP) image of the sample. (c) Photoacoustic MIP image. (d) Photoacoustic and ultrasound line profiles through the center of the sample. (Reproduced with permission of the authors and publishers.)

percutaneous radiofrequency ablation (RFA) procedures. The RFA needle can be better visualized in PA imaging compared to the ultrasound imaging and can also be used to differentiate ablated tissue. The interstitial illumination can assist needle guidance several centimeters inside the tissue. Further investigations are needed to understand the applicability of the proposed method in visualizing ablated tissue located deep inside a liver.

References

[1] P.-A. Clavien, H. Petrowsky, M. L. DeOliveira, and R. Graf, "Strategies for safer liver surgery and partial liver transplantation," *New England Journal of Medicine*, vol. 356, no. 15, pp. 1545–1559, 2007.

[2] J. L. Hinshaw, M. G. Lubner, T. J. Ziemlewicz, F. T. Lee Jr, and C. L. Brace, "Percutaneous tumor ablation tools: microwave, radiofrequency, or cryoablationwhat should you use and why?" *Radiographics*, vol. 34, no. 5, pp. 1344–1362, 2014.

[3] L. S. Poulou, E. Botsa, I. Thanou, P. D. Ziakas, and L. Thanos, "Percutaneous microwave ablation vs radiofrequency ablation in the treatment of hepatocellular carcinoma," *World journal of hepatology*, vol. 7, no. 8, p. 1054, 2015.

[4] S. L. Wong, P. B. Mangu, M. A. Choti, T. S. Crocenzi, G. D. Dodd III, G. S. Dorfman, C. Eng, Y. Fong, A. F. Giusti, D. Lu *et al.*, "American society of clinical oncology 2009 clinical evidence review on radiofrequency ablation of hepatic metastases from colorectal cancer," *Journal of Clinical Oncology*, vol. 28, no. 3, pp. 493–508, 2009.

[5] G. D. Dodd, M. C. Soulen, R. A. Kane, T. Livraghi, W. R. Lees, Y. Yamashita, A. R. Gillams, O. I. Karahan, and H. Rhim, "Minimally invasive treatment of malignant hepatic tumors: at the threshold of a major breakthrough," *Radiographics*, vol. 20, no. 1, pp. 9–27, 2000.

[6] F. Izzo, V. Granata, R. Grassi, R. Fusco, R. Palaia, P. Delrio, G. Carrafiello, D. Azoulay, A. Petrillo, and S. A. Curley, "Radiofrequency ablation and microwave ablation in liver tumors: An update," *The Oncologist*, 2019.

[7] S. Mulier, Y. Miao, P. Mulier, B. Dupas, P. Pereira, T. de Baere, R. Lencioni, R. Leveillee, G. Marchal, L. Michel *et al.*, "Electrodes and multiple electrode systems for radiofrequency ablation: a proposal for updated terminology," *European radiology*, vol. 15, no. 4, pp. 798–808, 2005.

[8] S. Mulier, Y. Ni, J. Jamart, T. Ruers, G. Marchal, and L. Michel, "Local recurrence after hepatic radiofrequency coagulation: multivariate meta-analysis and review of contributing factors," *Annals of surgery*, vol. 242, no. 2, p. 158, 2005.

[9] K. J. Francis, B. Chinni, S. S. Channappayya, R. Pachamuthu, V. S. Dogra, and N. Rao, "Characterization of lens based photoacoustic imaging system," *Photoacoustics*, vol. 8, pp. 37–47, 2017.

[10] P. Beard, "Biomedical photoacoustic imaging," *Interface focus*, vol. 1, no. 4, pp. 602–631, 2011.

[11] K. J. Francis, B. Chinni, S. S. Channappayya, R. Pachamuthu, V. S. Dogra, and N. Rao, "Multiview spatial compounding using lens-based photoacoustic imaging system," *Photoacoustics*, vol. 13, pp. 85–94, 2019.

[12] J. L. Su, A. B. Karpiouk, B. Wang, and S. Y. Emelianov, "Photoacoustic imaging of clinical metal needles in tissue," *Journal of biomedical optics*, vol. 15, no. 2, p. 021309, 2010.

[13] D. Piras, C. Grijsen, P. Schutte, W. Steenbergen, and S. Manohar, "Photoacoustic needle: minimally invasive guidance to biopsy," *Journal of biomedical optics*, vol. 18, no. 7, p. 070502, 2013.

[14] S. L. Jacques, "Optical properties of biological tissues: a review," *Physics in Medicine & Biology*, vol. 58, no. 11, p. R37, 2013.

[15] S. Iskander-Rizk, P. Kruizinga, A. F. van der Steen, and G. van Soest, "Spectroscopic photoacoustic imaging of radiofrequency ablation in the left atrium," *Biomedical optics express*, vol. 9, no. 3, pp. 1309–1322, 2018.

[16] P. Lanka, K. Francis, H. Kruit, S. K. V. Sekar, A. Farina, R. Cubeddu, S. Manohar, and A. Pifferi, "Monitoring radiofrequency ablation of biological tissue using broadband time-resolved diffuse optical spectroscopy," in *Diffuse Optical Spectroscopy and Imaging VII*, vol. 11074. International Society for Optics and Photonics, 2019, p. 110742M.

[17] N. Dana, L. Di Biase, A. Natale, S. Emelianov, and R. Bouchard, "In vitro photoacoustic visualization of myocardial ablation lesions," *Heart Rhythm*, vol. 11, no. 1, pp. 150–157, 2014.

[18] J. Rebling, F. J. O. Landa, X. L. Deán-Ben, A. Douplik, and D. Razansky, "Integrated catheter for simultaneous radio frequency ablation and optoacoustic monitoring of lesion progression," *Optics letters*, vol. 43, no. 8, pp. 1886–1889, 2018.

[19] K. J. Francis and S. Manohar, "Photoacoustic imaging in percutaneous radiofrequency ablation: device guidance and ablation visualization," *Physics in Medicine & Biology*, 2019.

[20] E. Rascevska, F. K. Joseph, and S. Manohar, "Annular illumination photoacoustic probe for needle guidance in medical interventions," in *Opto-Acoustic Methods and Applications in Biophotonics IV*, vol. 11077. International Society for Optics and Photonics, 2019, p. 110770L.

[21] K. J. Francis and S. Manohar, "Photoacoustic assisted device guidance and thermal lesion imaging for radiofrequency ablation," in *Opto-Acoustic Methods and Applications in Biophotonics IV*, vol. 11077. International Society for Optics and Photonics, 2019, p. 1107715.

[22] T. Gould, Q. Wang, and T. J. Pfefer, "Optical-thermal light-tissue interactions during photoacoustic breast imaging," *Biomedical optics express*, vol. 5, no. 3, pp. 832–847, 2014.

[23] J. Kim, S. Park, Y. Jung, S. Chang, J. Park, Y. Zhang, J. F. Lovell, and C. Kim, "Programmable real-time clinical photoacoustic and ultrasound imaging system," *Scientific reports*, vol. 6, p. 35137, 2016.